Diffuson-driven ultralow thermal conductivity in amorphous Nb_2O_5 thin films

Zhe Cheng,[1] Alex Weidenbach,[2] Tianli Feng,[3,4] M. Brooks Tellekamp,[2] Sebastian Howard,[5] Matthew J. Wahila,[5] Bill Zivasatienraj,[2] Brian Foley,[1] Sokrates T. Pantelides,[3,4] Louis F. J. Piper,[5,6] William Doolittle,[2] and Samuel Graham[1,7,*]

[1]*George W. Woodruff School of Mechanical Engineering, Georgia Institute of Technology, Atlanta, Georgia 30332, USA*
[2]*School of Electrical and Computer Engineering, Georgia Institute of Technology, Atlanta, Georgia 30332, USA*
[3]*Department of Physics and Astronomy and Department of Electrical Engineering and Computer Science, Vanderbilt University, Nashville, Tennessee 37235, USA*
[4]*Materials Science and Technology Division, Oak Ridge National Laboratory, Oak Ridge, Tennessee 37831, USA*
[5]*Department of Physics, Applied Physics and Astronomy, Binghamton University, Binghamton, New York 13902, USA*
[6]*Materials Science and Engineering, Binghamton University, Binghamton, New York 13902, USA*
[7]*School of Materials Science and Engineering, Georgia Institute of Technology, Atlanta, Georgia 30332, USA*

(Received 30 July 2018; revised manuscript received 4 December 2018; published 21 February 2019)

Niobium pentoxide (Nb_2O_5) has been investigated extensively for applications such as electrochemical energy storage, memristors, solar cells, light emitting diodes, and electrochromic devices. The thermal properties of Nb_2O_5 play a critical role in device performance of these applications. However, very few studies on the thermal properties of Nb_2O_5 have been reported and a fundamental understanding of heat transport in Nb_2O_5 is still lacking. The present paper closes this gap and provides a study of thermal conductivity of amorphous Nb_2O_5 thin films. Ultralow thermal conductivity is observed without any size effect in films as thin as 48 nm, which indicates that propagons contribute negligibly to the thermal conductivity and that the thermal transport is dominated by diffusons. By using the vibrational density of states of the single-crystal phase obtained from density functional theory simulations as an approximation, a diffuson-mediated minimum thermal conductivity model confirms this finding. Additionally, the measured thermal conductivity is lower than the amorphous limit, which proves that the diffuson model works better than the amorphous limit model to describe the thermal conduction mechanism in the amorphous Nb_2O_5 thin films. Additionally, the thermal conductivity does not change significantly with oxygen vacancy concentration. This stable and low thermal conductivity facilitates excellent performance for applications such as memristors.

DOI: 10.1103/PhysRevMaterials.3.025002

I. INTRODUCTION

Niobium pentoxide (Nb_2O_5) has been used extensively for applications such as electrochemical energy storage [1–5], solar cells and light emitting diodes (LEDs) [6–9], electrochromic devices [10,11], and memristors [12–14]. Thermal management in electrochemical energy-storage devices such as batteries and supercapacitors, solar cells, and LEDs is critical for device performance, reliability, and safety [15–17]. For electrochromic applications, such as smart windows, thermal insulation plays an important role in building energy savings [10]. For memristors, the electrical properties are directly related to the local temperature field and thermal insulation is a key for reducing device power consumption [18–20]. However, very few experimental studies on the thermal properties of Nb_2O_5 have been performed and a fundamental understanding of heat transport in this material, especially the amorphous state, is still lacking. In amorphous materials, heat is carried by local vibrations (locons), standing nonlocalized vibrations (diffusons), and propagating vibrations (propagons) [21], while the phonon gas model which is based on vibrations in an infinitely large and pure crystal is still extensively used in applications [11,22,23]. Some amorphous materials like amorphous silicon show a size effect in their thermal conductivity because propagons are a major contributor, while some others like amorphous SiO_2 do not as their thermal transport is dominated by diffusons [24,25]. It is interesting and important to explore how heat carriers contribute to thermal conductivity of Nb_2O_5 for both fundamental understanding and practical applications [13,17,19,22,23,26].

In this paper, we report the thermal conductivity of amorphous Nb_2O_5 thin films. Time-domain thermoreflectance (TDTR) is used to measure the thermal conductivity of these thin films and DFT simulations are used to calculate the vibrational properties of single-crystal Nb_2O_5. A diffuson-mediated minimum thermal conductivity model is used to interpret the measured thermal conductivity. Additionally, the effects of oxygen-vacancy concentration, thickness, and temperature on the thermal conductivity of amorphous Nb_2O_5 are studied.

II. METHODS

Nb_2O_5 films were deposited on sapphire substrates by room-temperature reactive dc sputtering using a Nb target in an ambient oxygen environment. Oxygen flow and process pressure were kept constant at 15 sccm and 10 mTorr,

*Corresponding author: sgraham@gatech.edu

respectively. Niobium power levels were varied from 25 to 50 W to tune the Nb:O ratio, producing films with different oxygen vacancy concentrations. The thicknesses of these films were measured using a Tencor P15 profilometer for films with a thickness larger than 200 nm. X-ray reflectivity (XRR) measurements were taken for films with a thickness less than 200 nm. XRR measurements were taken with a Panalytical X'Pert MRD Pro using a double crystal detector and a Cu Kα1 x-ray source. Grazing angle scans were taken using a $1/4°$ slit on the detector and a $1/4°$ slit on the source.

To obtain the structure information of these films, x-ray diffraction (XRD) measurements were taken with a Panalytical X'Pert MRD Pro using a double crystal detector and a Cu Kα1 x-ray source. Symmetric 2Θ-ω scans were taken using a $1/4°$ slit on the detector and a $1/4°$ slit on the source. Additionally, to obtain the oxygen vacancy concentration (i.e., compositions) of the Nb_2O_5 films, x-ray photoelectron spectroscopy (XPS) measurements were done at room temperature under ultrahigh vacuum ($\sim 10^{-7}$ Pa) using a monochromated Al-Kα source (1486.6 eV). Ar ion and electron flood guns were used to neutralize sample charging during measurement. Binding-energy calibration was performed using an internal adventitious carbon reference (C 1*s* at 284.8 eV) and external Au foil reference in electrical contact with the films. More details can be found in Ref. [27].

The thermal conductivity of these Nb_2O_5 thin films in this paper was measured by TDTR. TDTR is an optical pump and probe method which can be used to measure thermal properties of both nanostructured and bulk materials. An ultrafast pump laser beam periodically heats the sample surface while a delayed probe laser beam detects the temperature decay of the sample surface via a change in reflectivity recorded by a photodiode and a lock-in amplifier. The decay curve is fit to a multilayer thermal model to infer unknown thermal properties. More details can be found in Refs. [28,29]. To obtain the phonon properties of single-crystal Nb_2O_5, DFT calculations were performed using the VASP program package with the projector augmented wave method in the local density approximation [30–32]. The single-crystal Nb_2O_5 polytype studied is in the space group 12 ($C2/m$), with seven atoms per primitive cell. More details about the crystalline structure can be found in Supplemental Material [33]. The lattice structure was relaxed using the primitive unit cell with a convergence of 10^{-8} eV for the total energy, and 10^{-7} eV Å^{-1} for the forces on each atom. The plane-wave energy cutoff was 500 eV. The electronic k-space integration was performed with the tetrahedron method using a Γ-centered $9 \times 9 \times 15$ k mesh. The phonon dispersion is calculated via $3 \times 3 \times 3$ primitive cells (189 atoms) by the finite difference method implemented in the PHONOPY package with a Γ-centered $3 \times 3 \times 5$ k mesh [34].

III. RESULTS AND DISCUSSION

A. Sample structure

The oxygen-vacancy concentrations of these Nb_2O_5 thin films grown on sapphire substrates were varied by modifying the Nb target power with respect to a constant oxygen pressure. As such, the films are henceforth referred to as Nb_2O_{5-x}

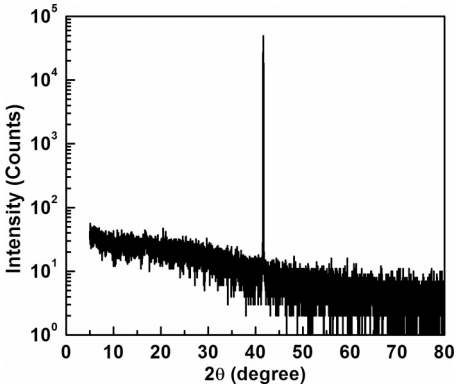

FIG. 1. The XRD pattern of a Nb_2O_5 film with 50-nm thickness and 45-W growth power.

where x represents the deviation from a stoichiometric oxygen content (oxygen vacancies). The thin films were characterized by XRD. Figure 1 shows the XRD pattern of a Nb_2O_5 film with 50-nm thickness and 45-W growth power as an example to demonstrate the films are amorphous. The peak in the XRD pattern is from the sapphire substrate. Other films with different thicknesses were checked by XRD as well to confirm all of them are amorphous.

XPS was used to determine the ratio of Nb and O atoms in the films [27]. The Nb:O ratios of films with different growth powers are shown in Table I. Each reported ratio is an average of 17 measurements taken on different sample spots. The given error bars are the statistical variations of the 17 measured spots for each sample. The surface oxygen component in the O 1*s* core level was subtracted. All the grown films are oxygen deficient compared to stoichiometry (common for most amorphous metal oxides) and the Nb:O ratio increases slightly with the growth power.

B. Phonon properties of single-crystal Nb_2O_5

DFT calculations of the phonon properties of single-crystal Nb_2O_5 with space group $C2/m$ (seven atoms per unit cell) have been performed. These calculations will be useful in our study of thermal transport in amorphous Nb_2O_5 later in the paper. Because it is very difficult to obtain the vibrational density of states (DOS) of amorphous materials, here we use the phonon DOS of single-crystal materials as an approximation. More details will be discussed later. The phonon dispersion relation and phonon DOS are shown in Figs. 2(a) and 2(b). The small negative frequency near zone center is some limitation of the numerical calculation. To further check the elastic stability of the crystal, we calculated the elastic moduli matrix. The six leading principal minors, or six nested principal minors, of the elastic moduli matrix are positive. This shows the material is stable. More details can be found in Supplemental Material [33]. Since the zone-center

TABLE I. Nb:O ratios of thin films with different growth powers.

Growth power	30 W	40 W	50 W
Nb:O ratio	0.481 (±0.027)	0.482 (±0.021)	0.497 (±0.018)

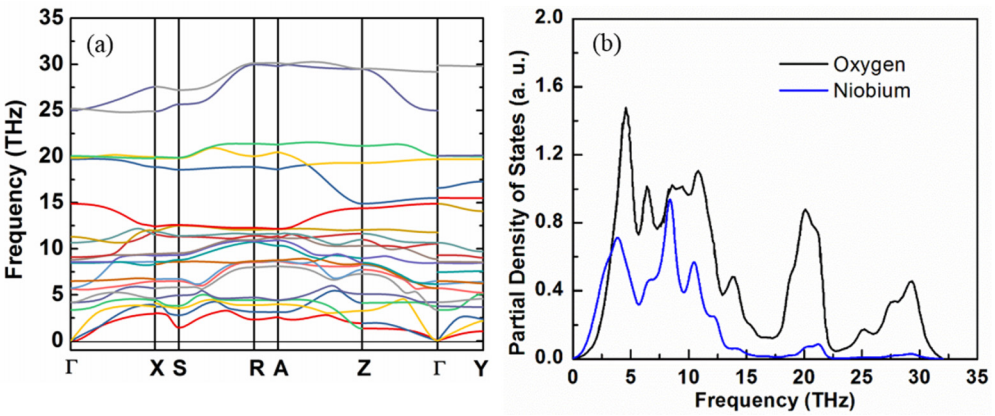

FIG. 2. DFT calculated (a) phonon dispersion relation and (b) partial phonon density of states of Nb_2O_5.

phonon DOS is small and negligible for the thermal transport modeling in the paper, the small negative frequency near zone center does not affect the following results. As shown in Fig. 2(a), the asymmetric complex crystal structure leads to a large number of optical phonon branches. Optical phonons contribute to thermal conductivity very differently for different materials [35]. The large amount of optical phonons in Nb_2O_5 scatter extensively with acoustic phonons, leading to a small phonon-phonon scattering relaxation time and subsequently low thermal conductivity. There is no phonon band gap between the low-frequency optical phonons (3–12 THz) and acoustic phonons, resulting in extensive interactions between optical and acoustic phonons, which reduce thermal conductivity. Taking the Γ-X direction, for example, two phonon band gaps (15–18 and 20–24 THz) are observed. These high-frequency optical phonons are less likely to interact with acoustic phonons than the low-frequency optical phonons. Correspondingly, there are two DOS valleys at these frequency ranges in Fig. 2(b). It is noteworthy that niobium contributes very little to the high-frequency DOS.

The overall phonon DOS is projected to Nb and O species in Fig. 2(b). The total area enclosed by the partial DOS of oxygen is 2.5 times that of niobium since oxygen is 2.5 times the stoichiometric amount of Nb. For frequencies larger than 15 THz, the optical phonon branches come from oxygen vibrations because of the small atomic mass of oxygen. In the acoustic-phonon frequency range (0–3 THz), the DOS contributed by niobium is larger than that by oxygen. Heavy atoms dominate in low-frequency acoustic vibrations and contribute to thermal conductivity. For high frequencies (>13 THz), we can see from Fig. 2(b), the DOS contributed by niobium is almost zero. According to the phonon dispersion relation in Fig. 2(a), we determine the average phonon group velocity of Nb_2O_5 to be approximately 5000 m s^{-1}, which is very close to the sound velocity obtained from the picosecond acoustic method in TDTR measurements.

The temperature-dependent Helmholtz free energy, entropy, and heat capacity of single-crystal Nb_2O_5 have also been calculated and reported in Fig. 3. The relation between Helmholtz free energy (F) and entropy (S) is $S = -\partial F/\partial T$. The Helmholtz free energy and entropy are of great significance in the calculation of thermodynamical properties, such as the thermal expansion coefficient. The heat capacity is compared with measured values in the literature and excellent agreement is achieved [36]. As the temperature increases, more high-energy phonon modes are excited, resulting in an increasing heat capacity. At high temperatures (>500 K), all the phonon modes are fully excited, resulting in a constant heat capacity. The heat-capacity values shown here are used in the TDTR data fittings.

C. Effects of thickness and growth power on thermal conductivity

In this paper, multifrequency TDTR measurements were used to measure the thermal properties of the Nb_2O_{5-x} films. A layer of Al (~80 nm) was deposited on the Nb_2O_{5-x} films as TDTR transducers. Figures 4(a)–4(c) show the TDTR sensitivity of different to-be-measured parameters with different modulation frequencies (2.2, 3.6, and 6.3 MHz). The definition of TDTR sensitivity is

$$S_i = \frac{\partial \ln(-V_{\text{in}}/V_{\text{out}})}{\partial \ln(p_i)}, \tag{1}$$

where S_i is the sensitivity to parameter i, $-V_{\text{in}}/V_{\text{out}}$ is the TDTR signal, and p_i is the value of parameter i [28]. The TDTR sensitivities of the thermal conductivity of Nb_2O_5 (κ_{Nb2O5}), the thermal boundary conductance of

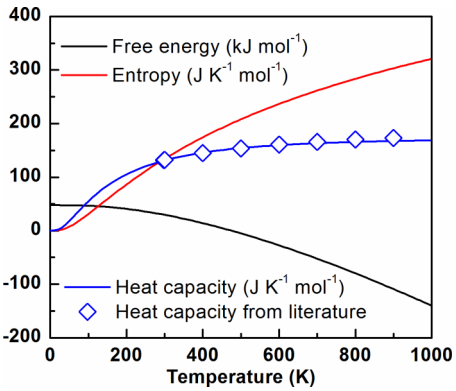

FIG. 3. DFT-calculated heat capacity, Helmholtz free energy, and entropy of single-crystal Nb_2O_5. The calculated heat capacity is compared with measured values in the literature [36].

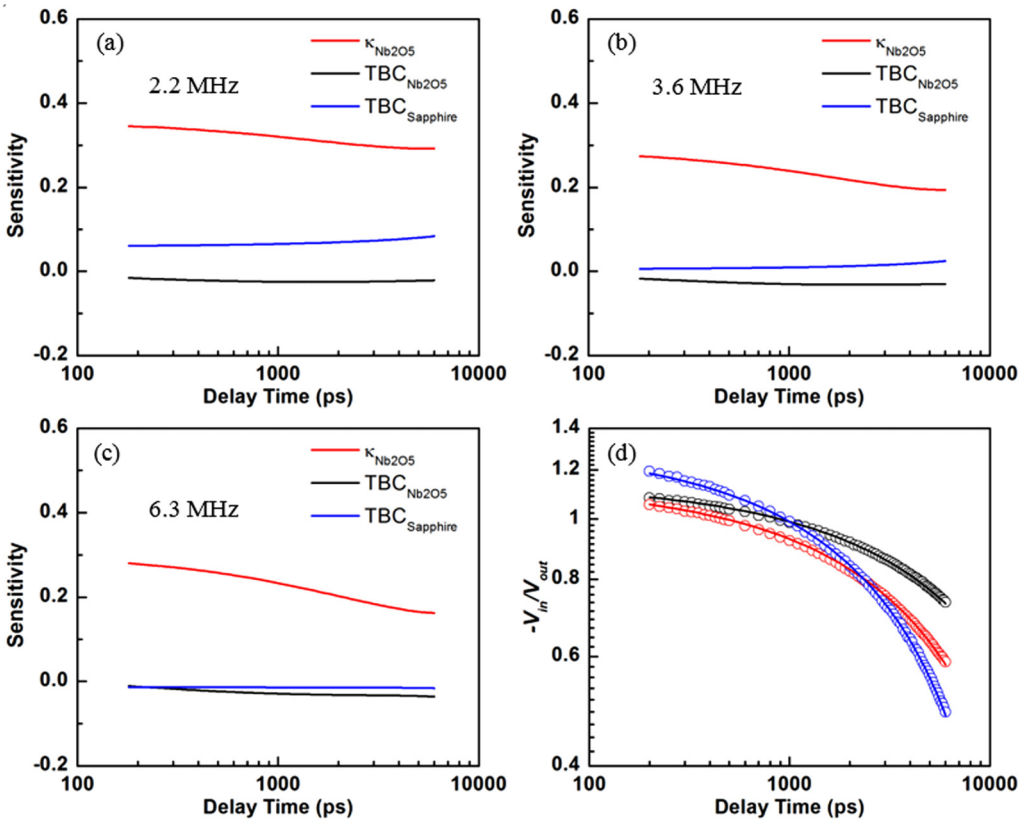

FIG. 4. (a)–(c) TDTR sensitivity of thermal conductivity of Nb_2O_5 (κ_{Nb2O5}), thermal boundary conductance of Al-Nb_2O_5 (TBC_{Nb2O5}), and thermal boundary conductance of Nb_2O_5-sapphire ($TBC_{sapphire}$) with different TDTR modulation frequencies. (d) Multifrequency TDTR data fitting. Circles represent experimental data while lines represent fitting data. Black, red, and blue represent data with modulation frequency of 2.2, 3.6, and 6.3 MHz.

Al-Nb_2O_5 (TBC_{Nb2O5}), and the thermal boundary conductance of Nb_2O_5-sapphire ($TBC_{sapphire}$) are all shown in Figs. 4(a)–4(c). The sensitivity of the thermal conductivity of Nb_2O_5 is very large, which is excellent for TDTR measurements. The pump and probe beam sizes are 7.7 and 7.5 μm (radii). Figure 4(d) shows an example of the excellent experimental and theoretical data fitting of TDTR measurements of 300-nm Nb_2O_5 thin films with growth power of 45 W. For the parameters in the data fitting, the thickness of Al is measured with the picosecond-acoustic method. The thermal conductivity of the Al layer is determined by measuring its electrical conductivity and applying the Wiedemann-Franz law. The other parameters are from the literature [28,37–39]. A silicon reference sample is checked every time before TDTR measurements to make sure that the TDTR system works well.

The effects of thickness and growth power on the measured thermal conductivity of Nb_2O_{5-x} films are shown in Fig. 5. The thermal conductivity was measured for Nb_2O_{5-x} films with thicknesses as low as 48 nm. The thermal conductivity is around $1\,W\,m^{-1}\,K^{-1}$ regardless of thickness (no size effect). The present paper serves as a benchmark for the thermal properties of amorphous Nb_2O_{5-x} films, which are needed for multiphysics modeling in memristors and other applications [20,40,41]. Moreover, the thickness-dependent thermal conductivity data show that Nb_2O_{5-x} is different from amorphous silicon or SiC in which propagons contribute a large fraction of the thermal conductivity [24,42–44]. In Nb_2O_{5-x}, no thickness dependence is observed, which indicates that propagons contribute negligibly to the thermal conductivity of these films. Therefore, we conclude that diffusons dominate the thermal transport in amorphous Nb_2O_{5-x} thin films.

Similar to thickness, the data show that growth power does not affect the thermal conductivity of Nb_2O_{5-x} films either. The growth power is correlated to oxygen vacancy concentration in the films, as shown in Table I. The growth power of the Nb target determines the amount of released Nb from the target while the oxygen pressure is constant. The higher the grown power is, the larger amount of Nb is released. As a result, the Nb:O ratios, and subsequently oxygen vacancy concentrations, are varied with growth powers. The samples grown with higher growth powers have higher oxygen-vacancy concentrations. However, these vacancies do not affect the thermal conductivity because the lattice vibrations in the films are localized (locons) or short-range propagated (diffusons). Locons usually contribute very little to thermal conductivity because they do not propagate and they transport heat [25,43]. Diffusons dominate heat transport in these films. Unlike phonons in crystalline materials, both locons and diffusons are not sensitive to point defects like oxygen vacancies in the films

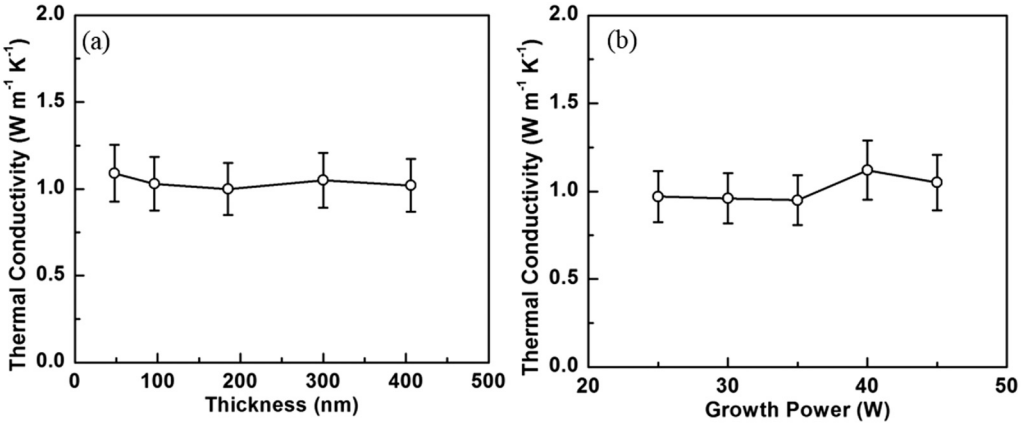

FIG. 5. (a) Effect of film thickness on thermal conductivity. (b) Effect of growth power on thermal conductivity.

because the amorphous films themselves are disordered [45].

D. Diffuson-driven ultralow thermal conductivity

The temperature-dependent thermal conductivity of Nb_2O_{5-x} films has also been measured by TDTR to explore the thermal conduction mechanism. In amorphous materials, the concept of a phonon does not hold. The definition of phonon group velocity in the kinetic-theory-based phonon thermal conductivity $\mathcal{K} = C_v l v/3$ is not applicable either. By assuming the mean free paths of the Debye-like heat-carrying oscillations are half of the corresponding wavelengths, Cahill developed a minimum thermal conductivity model [46–48]:

$$\mathcal{K}_{\text{Cahill}} = \left(\frac{\pi}{6}\right)^{1/3} k_B n^{2/3} \sum_{i=1}^{3} v_i \left(\frac{T}{i}\right)^2 \int_0^{\Theta_i/T} \frac{x^3 e^x}{(e^x-1)^2} dx, \tag{2}$$

where k_B is the Boltzmann constant, v_i is the sound velocity of polarization i, n is the atomic density, $\Theta_i = v_i(h/2\pi k_B)(6\pi^2 n)^{1/3}$ is the cutoff frequency expressed as temperature unit (similar to Debye temperature for crystalline materials), and h is the Planck constant. The calculated values of this model are referred to as the amorphous limit.

The thermal conductivity can be expressed as $\mathcal{K} = \int_0^\infty g(\omega)C(\omega)D(\omega)d\omega$ to avoid the definition of phonon group velocity as well. Here, $g(\omega)$ is the density of states at frequency ω, $C(\omega)$ is the heat capacity, and $D(\omega)$ is the thermal diffusivity. Recently, by introducing a diffuson diffusivity, Agne *et al.* developed another minimum thermal conductivity model for diffuson-mediated thermal transport [49]:

$$\mathcal{K}_{\text{diffuson}} = \frac{n^{1/3}k_B}{\pi} \int_0^\infty \left(\frac{g(\omega)}{3n}\right)\left(\frac{h\omega}{2\pi T k_B}\right)^2 \times \frac{e^{\frac{h\omega}{2\pi T k_B}}}{\left(e^{\frac{h\omega}{2\pi T k_B}}-1\right)^2} \omega d\omega. \tag{3}$$

The only input in this model is the DOS $g(\omega)$, which is obtained from DFT calculations, as shown in Fig. 6(a). The direct calculation of the vibrational DOS of an amorphous material is not practical in DFT. We therefore use the single-crystal phase to approximate the amorphous material's DOS, since the two are usually similar [50]. Reference [49] is a good demonstration for silicon. For more general cases, the atomic mass and bonds among atoms are the same for amorphous and single-crystal phases. If we consider the lattice vibrations as a mass-spring system or harmonic oscillators, the mass and spring constant are the same for amorphous and single-crystal phases. As a result, the basic lattice vibrational properties are the same or similar for amorphous and single-crystal phases. For example, heat capacities of amorphous materials are usually close to their single-crystal counterparts. Heat capacity is determined directly by the vibrational density of states. If the vibrational density of states of the amorphous phase is very different from that of the single-crystal phase, the corresponding heat capacity will be very different. This is why the vibrational density of states of the single-crystal phase is used in the calculation of minimum thermal conductivity in both Ref. [48] and our paper. By inserting the DFT-calculated vibrational DOS into Eq. (3), the minimum thermal conductivity of diffuson-mediated thermal transport is obtained. It is notable that harmonic calculations are not able to calculate the thermal conductivities of crystalline materials, in which the phonon lifetime needs to be calculated from anharmonic lattice dynamics, but for amorphous materials DOS is enough to calculate the minimum thermal conductivity because minimum oscillation lifetimes are assumed. For example, the Cahill model assumes the oscillation lifetime as one half of the vibration period (the mean free paths are half of the corresponding wavelengths). Similar treatment is applied to the diffuson model as well.

As shown in Fig. 6(b), we show that the measured thermal conductivity of the Nb_2O_{5-x} films changes with temperature. The accuracy of the measurement is insufficient to determine the temperature dependency of thermal conductivity (decreasing or keeping constant with temperature). The measured thermal conductivity is lower than the amorphous limit (Cahill model), while the diffuson model captures the major contribution to the thermal conductivity. We can still see small discrepancy between the measured thermal conductivity and the values calculated by the diffuson model. One possible reason is the small difference between the DOS of amorphous and single-crystal phases. Another possible reason is the experimental error of the TDTR measurements. The error bars

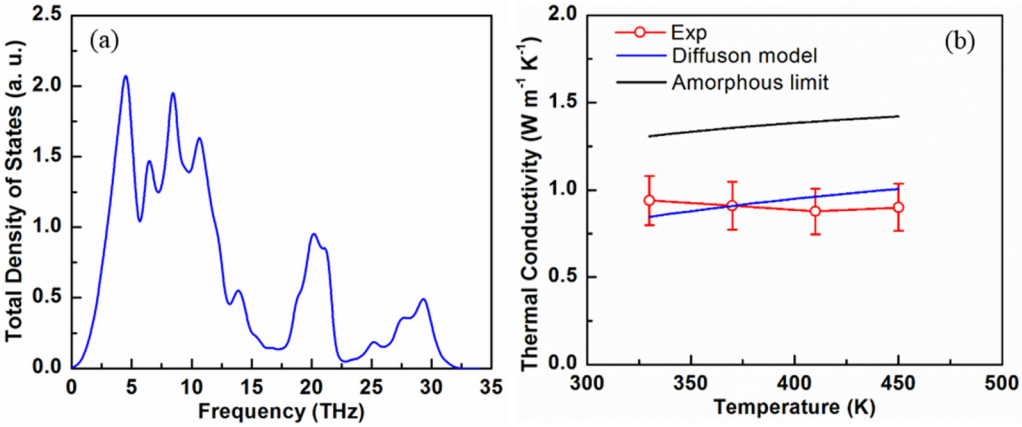

FIG. 6. (a) Total vibrational DOS from DFT calculation. (b) Temperature-dependent thermal conductivity. Two minimum thermal conductivity models are calculated to compare with the experimental values.

of the measured thermal conductivity reported in this paper are estimated as ±15%. The agreement between the measured thermal conductivity and the diffuson model is consistent with the conclusion in the last section that diffusons dominate the thermal transport. For memristor applications, the stable and ultralow thermal conductivity facilitates improved device performance by lowering the threshold voltage, threshold current, and device power consumption [20].

IV. CONCLUSION

To summarize, the present paper reported for the first time the thermal conductivity of amorphous Nb_2O_5 thin films with TDTR and obtained an ultralow thermal conductivity of $1\,W\,m^{-1}\,K^{-1}$. No size effect is observed in the measured thermal conductivity with film thickness as thin as 48 nm, indicating that propagons contribute negligibly to the thermal conductivity and the thermal transport is dominated by diffusons. By inputting DFT-calculated phonon DOS as an approximation of the vibrational DOS of the amorphous counterpart, a diffuson-mediated minimum thermal conductivity model confirms this finding. Additionally, the measured thermal conductivity is lower than the amorphous limit, which proves that the diffuson model works better than the amorphous limit model to describe the thermal conduction mechanism in the amorphous Nb_2O_5 thin films. It was also observed that the thermal conductivity does not change significantly with oxygen vacancy concentration. This stable and low thermal conductivity facilitates improved performance for applications such as memristors.

ACKNOWLEDGMENTS

This work is supported by the U.S. Department of Defense's Multidisciplinary University Research Initiatives Program "CEREBRAL" under Grant No. FA9550-18-1-0024. Theoretical calculations by T.L.F. and S.T.P. were supported in part by U.S. Department of Energy Grant No. DE-FG0209ER46554 and by the McMinn Endowment. Computations at Vanderbilt University and ORNL were performed at the National Energy Research Scientific Computing Center, a U.S. Department of Energy Office of Science User Facility funded through Contract No. DE-AC02-05CH11231. Computations also used the Extreme Science and Engineering Discovery Environment.

[1] M. Reddy, G. Subba Rao, and B. Chowdari, Chem. Rev. **113**, 5364 (2013).
[2] J. W. Kim, V. Augustyn, and B. Dunn, Adv. Ener. Mater. **2**, 141 (2012).
[3] V. Augustyn, J. Come, M. A. Lowe, J. W. Kim, P.-L. Taberna, S. H. Tolbert, H. D. Abruña, P. Simon, and B. Dunn, Nat. Mater. **12**, 518 (2013).
[4] X. Wang, G. Li, Z. Chen, V. Augustyn, X. Ma, G. Wang, B. Dunn, and Y. Lu, Adv. Ener. Mater. **1**, 1089 (2011).
[5] L. Yan, X. Rui, G. Chen, W. Xu, G. Zou, and H. Luo, Nanoscale **8**, 8443 (2016).
[6] R. Jose, V. Thavasi, and S. Ramakrishna, J. Am. Ceram. Soc. **92**, 289 (2009).
[7] J. Z. Ou, R. A. Rani, M. H. Ham, M. R. Field, Y. Zhang, H. Zheng, P. Reece, S. Zhuiykov, S. Sriram, M. Bhaskaran, and R. B. Kaner, ACS Nano **6**, 4045 (2012).
[8] E. Barea, X. Xu, V. González-Pedro, T. Ripollés-Sanchis, F. Fabregat-Santiago, and J. Bisquert, Ener. Env. Sci. **4**, 3414 (2011).
[9] J.-C. Su, C.-L. Lu, and C.-W. Chu, Appl. Opt. **48**, 4942 (2009).
[10] R. Baetens, B. P. Jelle, and A. Gustavsen, Solar Ener. Mater. Solar Cells **94**, 87 (2010).
[11] R. A. Rani, A. S. Zoolfakar, A. P. O'Mullane, M. W. Austin, and K. Kalantar-Zadeh, J. Mater. Chem. A **2**, 15683 (2014).
[12] M. D. Pickett, G. Medeiros-Ribeiro, and R. S. Williams, Nat. Mater. **12**, 114 (2013).
[13] M. Hota, M. Bera, S. Verma, and C. Maiti, Thin Solid Films **520**, 6648 (2012).
[14] C. Nico, T. Monteiro, and M. Graça, Progress in Mater. Sci. **80**, 1 (2016).
[15] A. L. Moore and L. Shi, Mater. Today **17**, 163 (2014).

[16] J. Cho, M. D. Losego, H. G. Zhang, H. Kim, J. Zuo, I. Petrov, D. G. Cahill, and P. V. Braun, Nat. Commun. **5**, 4035 (2014).
[17] Z. Rao and S. Wang, Renew. Sustain. Ener. Rev. **15**, 4554 (2011).
[18] R. Jiang, E. X. Zhang, S. E. Zhao, D. M. Fleetwood, R. D. Schrimpf, R. A. Reed, M. L. Alles, J. C. Shank, M. B. Tellekamp, and W. A. Doolittle, IEEE Trans. Nuclear Sci. **65**, 78 (2018).
[19] G. A. Gibson, S. Musunuru, J. Zhang, K. Vandenberghe, J. Lee, C. C. Hsieh, W. Jackson, Y. Jeon, D. Henze, Z. Li, and R. Stanley Williams, Appl. Phys. Lett. **108**, 023505 (2016).
[20] Z. Wang, S. Kumar, H.-S. P. Wong, and Y. Nishi, Appl. Phys. Lett. **112**, 073102 (2018).
[21] P. B. Allen, J. L. Feldman, J. Fabian, and F. Wooten, Philosoph. Magaz. B **79**, 1715 (1999).
[22] H. R. Seyf, L. Yates, T. L. Bougher, S. Graham, B. A. Cola, T. Detchprohm, M. H. Ji, J. Kim, R. Dupuis, W. Lv, and A. Henry, NPJ Comput. Mater. **3**, 49 (2017).
[23] W. Lv and A. Henry, Sci. Rep. **6**, 37675 (2016).
[24] J. L. Braun, C. H. Baker, A. Giri, M. Elahi, K. Artyushkova, T. E. Beechem, P. M. Norris, Z. C. Leseman, J. T. Gaskins, and P. E. Hopkins, Phys. Rev. B **93**, 140201 (2016).
[25] L. Yang, Q. Zhang, Z. Cui, M. Gerboth, Y. Zhao, T. T. Xu, D. G. Walker, and D. Li, Nano Lett. **17**, 7218 (2017).
[26] M. D. Pickett and R. S. Williams, Nanotechnol. **23**, 215202 (2012).
[27] J. C. Shank, M. B. Tellekamp, and W. A. Doolittle, Sci. Rep. **8**, 12935 (2018).
[28] Z. Cheng, T. Bougher, T. Bai, S. Y. Wang, C. Li, L. Yates, B. M. Foley, M. Goorsky, B. A. Cola, F. Faili, and S. Graham, ACS Appl. Mater. Interf. **10**, 4808 (2018).
[29] D. G. Cahill, Rev. Sci. Instrum. **75**, 5119 (2004).
[30] G. Kresse and J. Hafner, Phys. Rev. B **47**, 558 (1993).
[31] G. Kresse and J. Furthmüller, Phys. Rev. B **54**, 11169 (1996).
[32] P. E. Blöchl, Phys. Rev. B **50**, 17953 (1994).
[33] See Supplemental Material at http://link.aps.org/supplemental/10.1103/PhysRevMaterials.3.025002 for the crystal structure of single-crystal Nb_2O_5 and the elastic moduli matrix.
[34] A. Togo, F. Oba, and I. Tanaka, Phys. Rev. B **78**, 134106 (2008).
[35] Z. Tian, K. Esfarjani, J. Shiomi, A. S. Henry, and G. Chen, Appl. Phys. Lett. **99**, 053122 (2011).
[36] K. Jacob, C. Shekhar, M. Vinay, and Y. Waseda, J. Chem. Engineer. Data **55**, 4854 (2010).
[37] S.-M. Lee, D. G. Cahill, and T. H. Allen, Phys. Rev. B **52**, 253 (1995).
[38] D. Ditmars, S. Ishihara, S. Chang, G. Bernstein, and E. West, J. Res. Natl. Bur. Stand **87**, 159 (1982).
[39] A. M. Hofmeister, Phys. Chem. Miner. **41**, 361 (2014).
[40] C. Funck, S. Menzel, N. Aslam, H. Zhang, A. Hardtdegen, R. Waser, and S. Hoffmann-Eifert, Adv. Electron. Mater. **2**, 1600169 (2016).
[41] S. K. Nandi, X. Liu, D. K. Venkatachalam, and R. G. Elliman, J. Phys. D **48**, 195105 (2015).
[42] J. Moon, B. Latour, and A. J. Minnich, Phys. Rev. B **97**, 024201 (2018).
[43] J. M. Larkin and A. J. H. McGaughey, Phys. Rev. B **89**, 144303 (2014).
[44] S. Kwon, J. Zheng, M. C. Wingert, S. Cui, and R. Chen, ACS Nano **11**, 2470 (2017).
[45] M. N. Luckyanova, D. Chen, W. Ma, H. L. Tuller, G. Chen, and B. Yildiz, Appl. Phys. Lett. **104**, 061911 (2014).
[46] D. G. Cahill, S. K. Watson, and R. O. Pohl, Phys. Rev. B **46**, 6131 (1992).
[47] J. C. Duda, P. E. Hopkins, Y. Shen, and M. C. Gupta, Phys. Rev. Lett. **110**, 015902 (2013).
[48] C. Chiritescu, D. G. Cahill, N. Nguyen, D. Johnson, A. Bodapati, P. Keblinski, and P. Zschack, Science **315**, 351 (2007).
[49] M. T. Agne, R. Hanus, and G. J. Snyder, Ener. Environ. Sci. **11**, 609 (2018).
[50] A. France-Lanord, S. Merabia, T. Albaret, D. Lacroix, and K. Termentzidis, J. Phys.: Condens. Matter **26**, 355801 (2014).